

Dipole Antenna Miniaturization using Single-Cell Metamaterial

Amir Jafargholi and Manouchehr Kamyab

Department of Electrical Engineering
K. N. Toosi University of Technology, P.O.Box 16315-1355. Tehran, Iran
Jafargholi@ee.kntu.ac.ir, Kamyab@kntu.ac.ir

Abstract — Miniaturized printed dipole antenna loaded with reactive elements is proposed. The reactive loading of the dipole is inspired by the epsilon-negative (ENG) and double negative (DNG) metamaterial (MTM) inclusions, which enable the loaded dipole to be compacted. The reactive loads are realized by two rake-shaped split ring resonators (SRRs) facing each other. Investigations reveal that the loaded dipole radiates at two separated bands depending on load locations. The new resonance frequencies are lower than the natural resonance frequency of the conventional half wavelength dipole. In this range of frequencies, the radiation efficiency of the composite antenna is high. In order to validate the simulation results, a prototype of the proposed printed dipole is fabricated and tested. The agreement between the simulated and measured results is quite good.

Index Terms — Loaded dipole, metamaterial.

I. INTRODUCTION

The increasing demands on compact multifunctional devices have necessitated the development of miniaturized/multi-frequency printed dipoles which can be integrated into familiar devices such as laptop computers and mobile phones. The typical difficulties encountered in designing compact antennas include narrow bandwidth, and low radiation efficiency. In order to achieve a good efficiency, considerable effort must be expended on the matching network. Other researchers have found that the bandwidth of the dipole antenna can be enhanced by loading the antenna with parallel lumped element circuits [1]. Over the last decade,

increasing demands for low profile multifunctional antennas have resulted in considerable interest by the electromagnetic research community in MTMs. Due to unique electromagnetic properties; MTMs have been widely considered in monopole and dipole antennas to improve their performance [2-5]. The applications of composite right/left handed (CRLH) structures to load the printed dipole have been investigated both numerically [6-8] and analytically [9]. However, the main drawbacks of this method are low gain and low efficiency. The use of transmission-line based MTMs to realize a tri-band monopole antenna has been recently investigated in [10]. However, the cross polarization levels of the proposed antenna in [10] are very high. It is also known that the antenna properties can be improved by covering the metal radiating parts or filling the antenna volume. For instance, the bandwidth of the microstrip patch antenna can be significantly improved by replacing the dielectric substrate with the magneto-dielectric one [11]. The effect of complex material coverings on the bandwidth of the antennas has been also investigated in [12].

In this paper, first, the effect of material inclusions embedded in a simple dipole antenna has been investigated. The numerical investigations result in some general conclusions regarding the effect of material inclusions on the dipole antenna performance. It is demonstrated that in contrast to the double-positive (DPS) and mu-negative (MNG) MTMs, ENG-, and DNG-MTM inclusions can provide miniaturization and multi-band performance. To practically realize this method, a compact printed dipole antenna is designed using reactive loading, which is inspired by ENG-MTM inclusions.

To this aim, a novel printed MTM element is proposed and successfully tested. The proposed MTM cell shows ENG behavior at around the antenna operating frequency. The dimensions of the proposed MTM cell is optimized to meet the specifications of the mobile bands (890.2MHz–914.8MHz, and 1710MHz–1784MHz) while maintaining its compact size. The antenna radiation efficiency at the first resonance frequency is significantly higher than those reported for other miniaturized dipoles in the literature [6-9]. It is worthwhile to point out here that the subject of single-cell MTM loading is not new and has been studied by other authors [10].

II. LOADED DIPOLE ANTENNA WITH MTM INCLUSIONS

The resonance frequencies of an original monopole/dipole are harmonics of the main resonant frequency ω_1 . However, omnidirectional radiation pattern distortion and low directivity are two major disadvantages associated with monopole/dipole antenna resonating at higher order harmonics ($\omega_m > \omega_1$) [5, 13]. In this section, a simple and intuitive rule for determining the beneficial filling material type for dipole antennas has been introduced. A dipole antenna loaded with cylindrical dispersive MTM inclusions is shown in Fig. 1. It is assumed that the MTM inclusions are embedded in the both arms of the dipole. Here, the Drude model [14] is used to simulate the MTM inclusions, since it can yield a negative real part of the permittivity/permeability over a wide frequency range. Depending on the MTM type either μ or ϵ (or both) obey the Drude model (plasma frequency $\omega_p = 1.8 \times 10^{10}$ rad/s and collision frequency $f_c = 0.2$ GHz) and are equal to one otherwise. The distance from the location of the MTM inclusions to the feed point is denoted as d_{MIF} . The behaviors of the loaded dipole as a function of the MTM type, the distance of the MTM inclusions from the antenna feed point, d_{MIF} , and inclusion width have been studied here.

The computation time for the DPS inclusion is about 10 minutes for all frequency points compared to about an hour for a DNG case using CST over a frequency range of 0 to 6GHz, while this time increased in CST for higher permittivity and permeability materials. (For a 3.2GHz dual core CPU with 2GByte RAM).

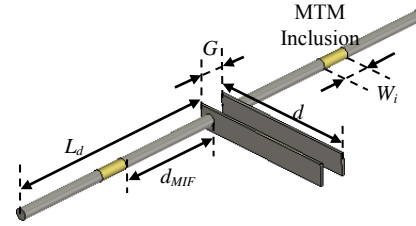


Fig. 1. An ideal model of MTM loaded dipole: $L_d=120$ mm, $W_i=2.5$ mm, $G=5$ mm, $d=27$ mm.

2.1. Power reflection coefficient, $|S_{11}|$ as a function of MTM distance from the antenna feed point

Figure 2, shows the antenna return loss for the dipoles loaded with DPS-, MNG-, DNG-, and ENG-inclusions, with d_{MIF} as a parameter. As the ENG- or DNG- inclusions are added, the antenna resonant behavior changes. It can be concluded from Fig. 2 that for the dipole antenna loaded with DNG- or ENG-inclusions, an additional resonance frequency is introduced at the frequencies lower than the antenna resonant frequency where the antenna radiates an omnidirectional radiation pattern. In contrast, for the dipoles loaded with DPS- or MNG-inclusions, changing DPS/MNG locations on the antenna arms causes no resonances at frequencies lower than the main resonance frequency, as shown in Figs. 2a and 2b. As the distance between the ENG-/DNG-inclusions and the feed point is increased, the main resonant frequency decreases while the low resonant frequency is almost unchanged. This feature provides the ability to choose the second resonance frequency arbitrarily based on provision dictated by application. Thus, the frequency ratio between these two frequencies can be readily controlled by adjusting the inclusion locations. In addition, for the case of the dipoles loaded with DNG-/ENG-blocks and $50\text{mm} < d_{MIF} < 75\text{mm}$, more than one resonance is introduced at around the antenna main resonant frequency where the antenna radiates omnidirectional radiation patterns, as shown in Figs. 2b and 2c. To make the concept clearer, three DNG loaded dipoles are designed and simulated. The return loss results for the dipole antennas loaded with different DNG blocks and different d_{MIF} are shown in Fig. 3. For comparison purposes, the power reflection coefficient of an unloaded dipole antenna is also presented in Fig. 3. As can be seen, all the antennas have multi-resonance behavior.

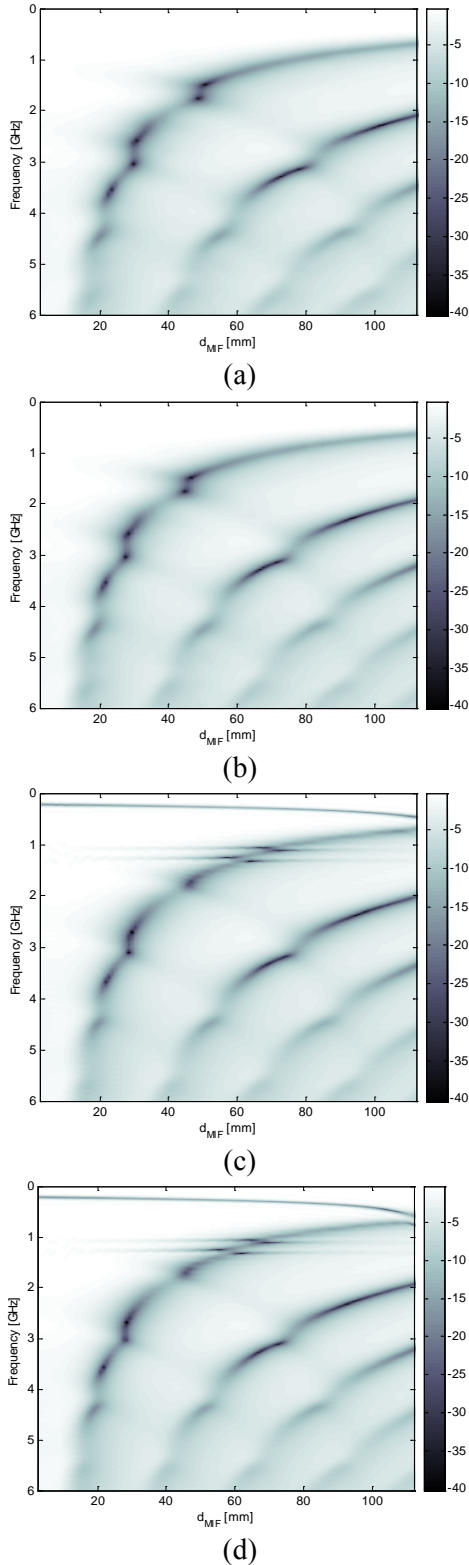


Fig. 2. CST Simulation Results for $|S_{11}|$ [dB], (a) DPS-, (b) MNG-, (c) DNG-, and (d) ENG-inclusions.

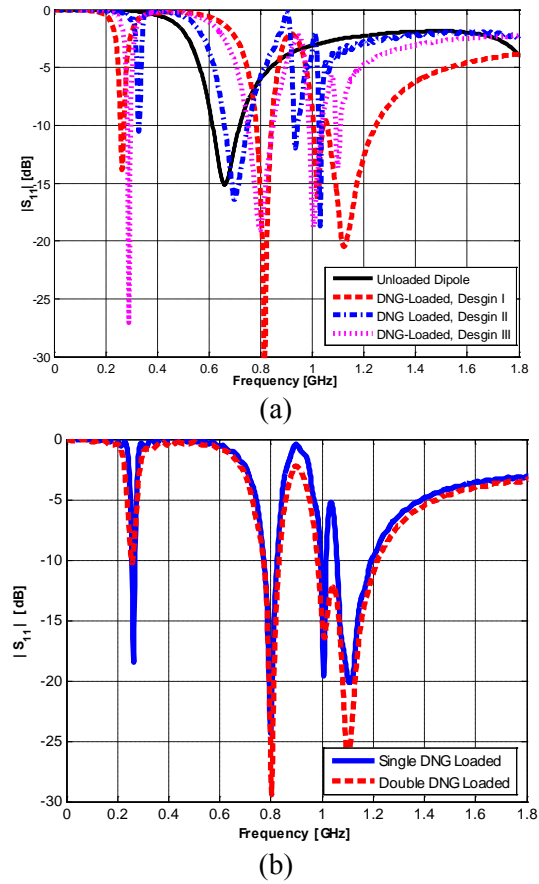


Fig. 3. Magnitude of S_{11} (a) of dipole antennas loaded with different DNG blocks, with Drude model and $\omega_p=1.8 \times 10^{10}$ rad/s; Design I: $d_{MIF}=72$ mm and, $f_c =0.2$ GHz, Design II: $d_{MIF}=100$ mm, $f_c =0.01$ GHz, and Design III: $d_{MIF}=85$ mm, $f_c =0.1$ GHz. As a reference, an unloaded dipole antenna is also simulated, (b) comparison for single and double loaded DNG materials: The first inclusions are located at $d_{MIF}=72$ mm while the second ones are located at the ends of the arms, $f_c=0.1$ GHz.

The first frequency bands of the proposed loaded dipoles are narrow. These narrow frequency bands are the direct consequence of the resonant nature of the MTM inclusions. The gain, efficiency, and bandwidth of the three loaded dipoles are compared in Table 1. For the first design, the antenna bandwidth at first resonance is quite good but its gain is low. In contrast, for the second design, the antenna has a high gain at the first resonance frequency but at the expense of a narrower bandwidth. As a result, the type of the

DNG-inclusion is a result of a trade-off between the antenna gain and bandwidth (Design III).

2.2. Power reflection coefficient, $|S_{11}|$ as a function of MTM type

In this section, the effects of two different cases of metamaterial inclusion have been investigated.

A. Non-dispersive materials

In Fig. 4, the effect of permittivity and permeability of DPS inclusion on the antenna resonance frequency has been studied. Increasing DPS load permittivity causes resonance frequency decreasing while, for the dipoles loaded with magnetic inclusions, changing permeability causes no resonance frequency change.

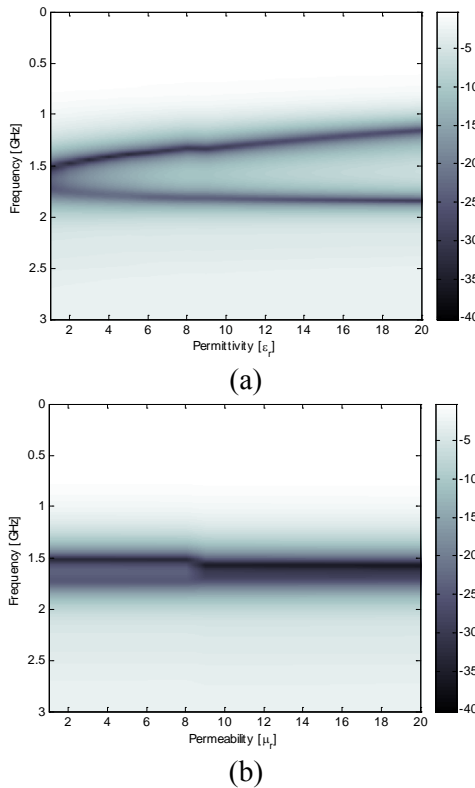


Fig. 4. CST simulation results for $|S_{11}|$ [dB], $d_{MIF}=45\text{mm}$, versus material (a) permittivity, $\mu_r=1$, and (b) permeability, $\epsilon_r=1$.

B. Dispersive materials

The behaviors of the loaded dipole as a function of the plasma frequency for $d_{MIF}=72\text{mm}$, have been studied. Figure 5 shows the antenna return loss for the dipoles loaded with ENG-, DNG-, and MNG-inclusions. It can be concluded from Fig. 5 that for a dipole antenna loaded with

DNG- or ENG-inclusions, an additional resonance frequency is introduced at the frequencies lower than the antenna resonant frequency.

As it seems in Fig. 5(b), in DNG-loaded case, an additional resonance occurs while compared with ENG inclusion. In contrast, for the dipoles loaded with MNG-inclusions, changing plasma frequency causes no resonances at lower frequencies, as shown in Fig. 5(c).

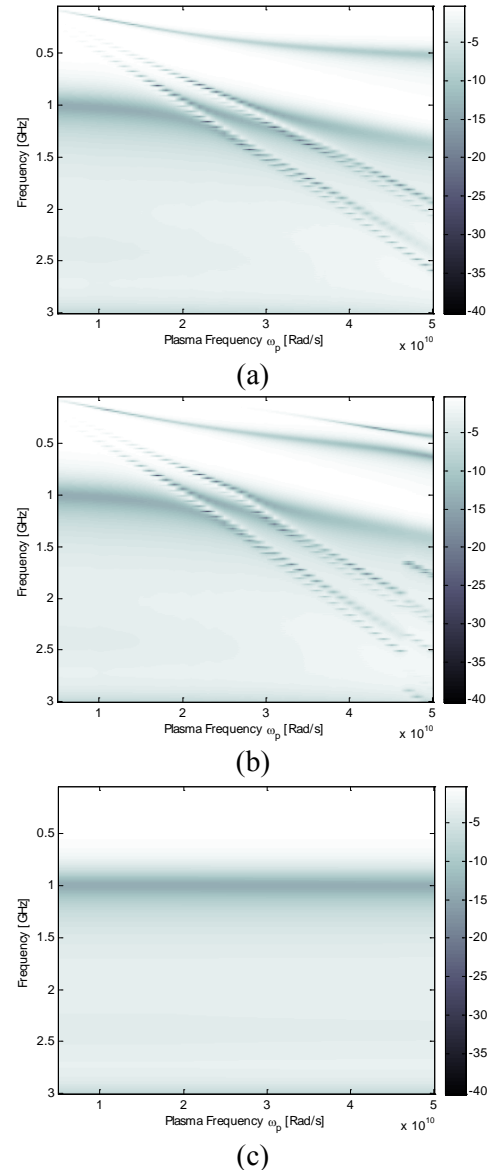


Fig. 5. CST simulation results for $|S_{11}|$ [dB] versus plasma frequency, $d_{MIF}=72\text{mm}$, (a) ENG-, (b) DNG-, (c) MNG-inclusions.

2.3. Power reflection coefficient, $|S_{11}|$ as a function of MTM width

The behaviors of the loaded dipole as a function of the inclusion width for $d_{MIF}=45\text{mm}$, have been studied. Figure 6 shows the antenna return loss for the dipoles loaded with DPS-, ENG-, DNG-, and MNG-inclusions. It can be concluded from Fig. 6 that for the dipole antenna loaded with DNG- or ENG-inclusions, an additional resonance frequency is introduced at the frequencies lower than the antenna resonant frequency. This resonance affects significantly by changing the width of MTM inclusion.

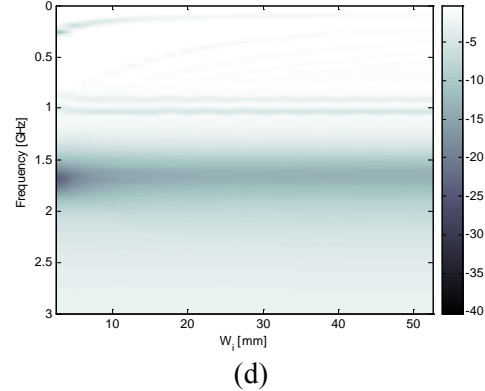
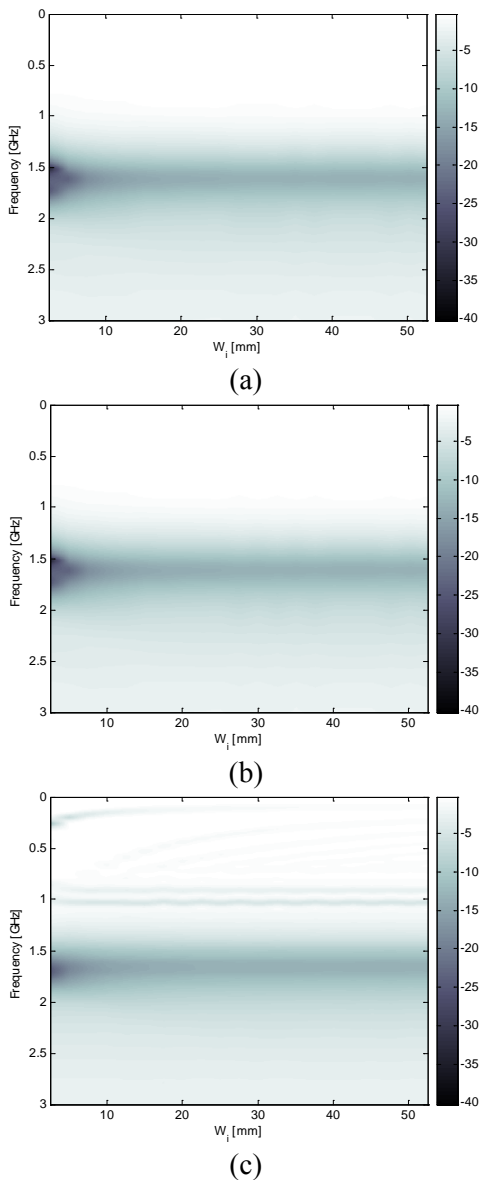


Fig. 6. CST simulation results for $|S_{11}|$ [dB], $d_{MIF}=45\text{mm}$, versus width of (a) DPS-, (b) MNG-, (c) DNG-, and (d) ENG-inclusions.

Decreasing the width causes more matching condition while increasing width of MTM inclusion makes antenna mismatching in this frequency. Again, in contrast, for the dipoles loaded with DPS- and MNG-inclusions, changing inclusion width causes no additional resonances at lower frequencies, as shown in Figs. 6(a) and 6(b).

III. PROPOSED METAMATERIAL CELL

In the previous section, it was revealed that the use of the ENG- and DNG-inclusions has led to a multi-resonance behavior. In this section, a new printed MTM cell is introduced to realize the ENG-inclusions. Figure 7 shows a schematic of the proposed MTM cell. The proposed MTM cell is printed on a FR4 substrate with a thickness of 0.8mm and a dielectric constant of 4.4. An important feature of the proposed MTM is that it offers more degrees of freedom than conventional MTM cells [14]. In order to retrieve the constitutive parameters of the proposed metamaterial, a unit cell positioned between two perfect electric conductors (PEC) in y direction and two perfect magnetic conductors (PMC) in x direction is simulated, and used to model an infinite periodic structure [15]. The resultant scattering parameters obtained from CST microwave studio are exerted to the Chen's algorithm [15]. Figure 8 shows the retrieved effective parameters of the proposed metamaterial cell. As can be seen, the proposed MTM cell has the permittivity that exhibits Drude behavior at frequencies lower than 1.1GHz and Lorentz behavior [14] at frequencies higher than 1.1GHz.

Thus, this MTM can be approximated via a combination of Lorentz and Drude models.

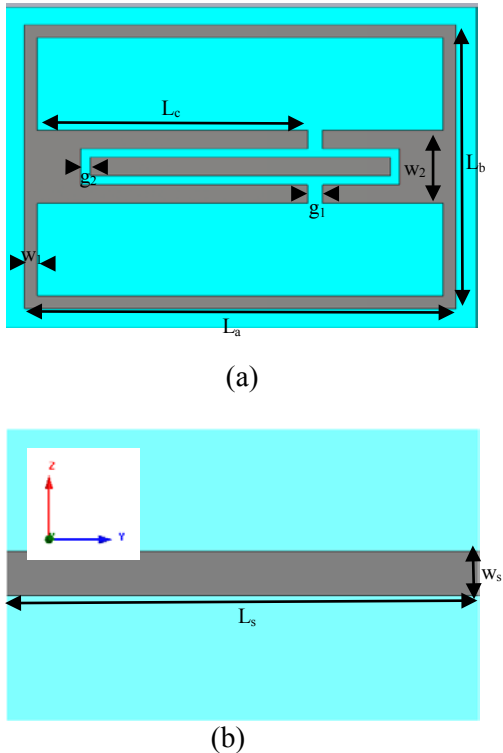


Fig. 7. Schematic of the proposed MTM unit cell and its design parameters, (a) front view, (b) back view: $L_a=23.54\text{mm}$, $L_b=15.55\text{mm}$, $L_c=14.78\text{mm}$, $w_1=0.7\text{mm}$, $g_1=0.8\text{mm}$, $w_2=4\text{mm}$, $g_2=0.5\text{mm}$, $w_s=2.5\text{mm}$, and $L_s=26.75\text{mm}$.

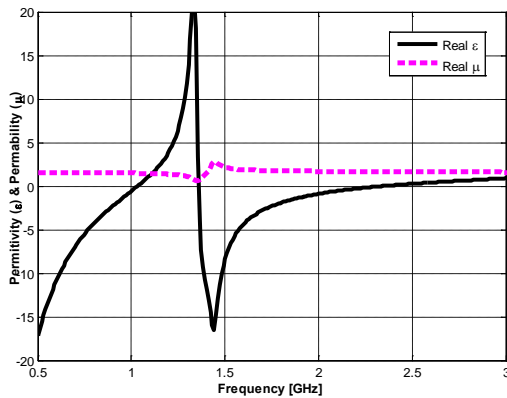


Fig. 8. Retrieved effective parameters of the proposed MTM cell.

IV. COMPACT DIPOLE ANTENNA

In order to realize the miniaturization method described in Section II, a double-sided printed dipole antenna is chosen for its simplicity in

implementation and its low profile. Figure 9(a) shows the proposed miniaturized printed dipole, in which a pair of proposed MTM cells is symmetrically added to each side of the printed dipole. The proposed MTM cells and dipole are printed on a FR4 substrate with a thickness of 0.8mm and a dielectric constant of 4.4 to reduce the cost of the antenna and to make it more rigid in construction.

For the MTM cells that are far away from the dipole arms, the coupling levels of them with the dipole arms are low and thus the arrangement of the several MTM cells has no effect on the frequency behaviour of the proposed antenna. As a result, the dipole is just loaded with single cell MTM. Similar to the DNG- [3] and ENG- [17] MTMs, the proposed MTM cell can be modelled as a parallel resonant LC circuit. Thus, the proposed metamaterial cell is modeled as a resonant LC circuit parallel to the dipole, and the radiation into the free space is modelled as a resistor [18]. A prototype of the proposed miniaturized dual-band printed dipole is fabricated to confirm the simulation results. Figure 9(b) shows a photograph of the fabricated antenna.

Figure 10 shows the return loss of the proposed symmetrically loaded dipole with the gap length, g_1 , of 0.8mm as well as the unloaded dipole antenna. As can be seen, the dipole antenna along with the loading elements provides good matching at both resonance frequencies. For comparison purposes, a simple dipole antenna loaded with lossy ENG inclusions, with the same retrieved effective parameters of the proposed MTM cell (Fig. 7), is also simulated. As can be seen from Fig. 10, the return loss of the dipole loaded with ENG inclusions correlates nicely to that obtained for the single cell MTM loaded dipole. The co-polarized and cross-polarized radiation patterns of the proposed loaded dipole are measured at the resonant frequencies of 940MHz and 1.7GHz. The measured and simulated radiation patterns at first and second resonant frequencies are shown in Fig. 11. As expected, the radiation patterns at both resonant frequencies are similar to that of the conventional unloaded dipole antenna.

The gain of the proposed antenna at a low resonant frequency is high compared to that of the other miniaturized MTM loaded dipoles [6-9]. The antenna gains at first and second resonant

frequencies are -2.679dBi and 1dBi, respectively. The proposed antenna has a broad bandwidth of 15.96% at 940MHz (which is significantly wider than the bandwidth of other miniaturized MTM loaded dipoles [6-9], [19-24]) and 32.35% at 1.7GHz. An important advantage of the proposed antenna is that the dipole length does not need to be increased to lower the resonant frequency. Consequently, a compact antenna is obtained.

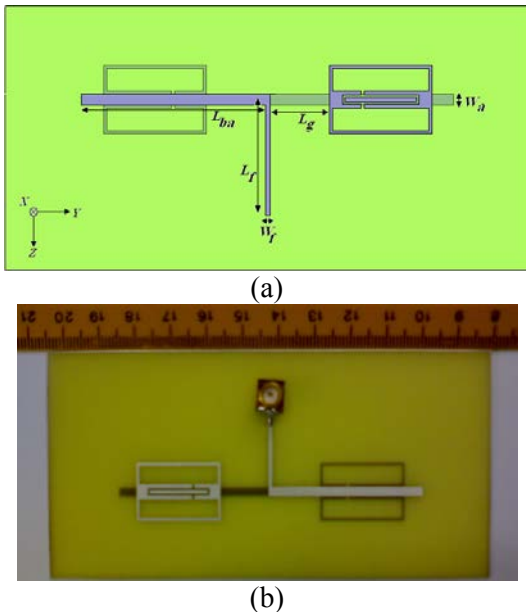


Fig. 9. (a) Printed dipole symmetrically loaded with single cell MTM: $L_{ba}=42.05\text{mm}$, $L_f=27.5\text{mm}$, $L_g=12.52\text{mm}$, $W_a=2.5\text{mm}$, $W_f=0.8\text{mm}$, and (b) prototype of proposed miniaturized printed dipole antenna loaded with single cell MTM.

Finally, the effect of the MTM location is investigated to obtain some engineering guidelines for loaded dipole designs. Thus, the loading elements move along the antenna arms and the antenna return loss is plotted in Fig. 12 for each stage. The gain, bandwidth and radiation efficiency of the loaded dipoles with different MTM locations are also compared in Table II. As can be seen, the first resonant frequency remains approximately unchanged while the second one reduces as the MTM cells move away from the antenna feed point. Thus, when the MTM elements move closer to the dipole ends the separation of the two resonances decreases. In addition, when the MTM cells are placed close to the antenna feed point, the proposed antenna cannot match very well to a 50Ω transmission line.

Moreover, as can be seen from Figs. 2 and 12, the single cell MTM loaded printed dipole follows closely the frequency behavior of the dipole antenna loaded with cylindrical dispersive ENG-inclusions, as d_{MIF} or L_g increases.

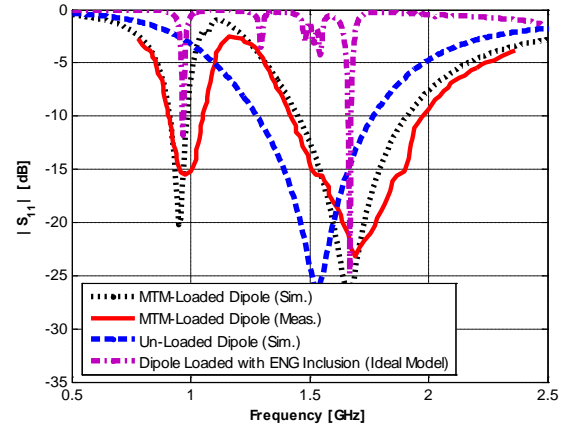


Fig. 10. Return loss of the proposed miniaturized printed dipole antenna loaded with single cell MTM. As a reference, an unloaded dipole and an ideal model of the ENG-Loaded dipole are also simulated.

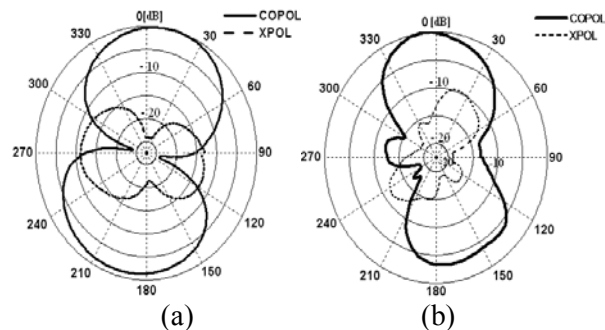


Fig. 11. Measured radiation patterns of the proposed antenna, (a) 940MHz and (b) 1.7GHz.

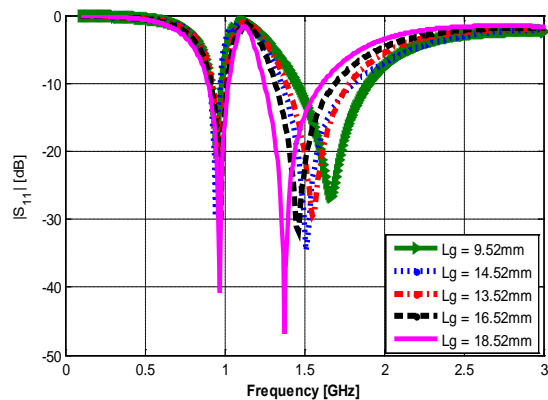


Fig. 12. The effect of the MTM location on the return loss of the printed dipole antenna.

Table 1: Gain, radiation efficiency, and bandwidth characteristics of the dipole antenna loaded with different DNG inclusions

L_g	Design I				Design II				Design III			
	f_{r1}	f_{r2}	f_{r3}	f_{r4}	f_{r1}	f_{r2}	f_{r3}	f_{r4}	f_{r1}	f_{r2}	f_{r3}	f_{r4}
f_0 (GHz)	0.26	0.8	1.0	1.1	0.33	0.7	0.93	1.0	0.29	0.8	1.0	1.1
Gain (dBi)	-7.2	1.25	0.0	2.1	1.3	2.1	1.9	3.4	-3.5	2.0	0.5	2.2
η (%)	12.2	78	65	91	84	99	100	100	25	91	80	95
BW (%)	5.6	7.5	5.4	21.8	1.1	13.1	2.4	1.5	4.5	12.1	5	1.8

Table 2: Comparison of the gain, bandwidth, and radiation efficiency for the loaded dipole antenna with different MTM Locations

L_g	9.52mm		13.52mm		14.52mm		16.52mm		18.52mm	
	f_{r1}	f_{r2}								
f_0 (GHz)	0.95	1.68	0.96	1.59	0.95	1.51	0.96	1.5	0.94	1.39
Gain (dBi)	-2.38	1	-2.3	0.7	-2.5	0.55	-2.36	0.3	-2.7	0.14
η (%)	88	93	97	94	90	93	92	92	87	93
BW (%)	8.1	27	9.7	27	8.9	27	11.5	25	7.3	21

IV. CONCLUSION

The behavior of a dipole antenna loaded with MTM inclusions has been examined. It has been revealed that embedding DNG-/ENG-inclusions in a simple dipole antenna can provide an opportunity to design miniaturized multi-band antenna. In order to realize this method, a single unit cell of MTM reactive loading has been utilized. Results show that placing proposed MTM cells in close proximity of a printed dipole antenna creates a double resonant antenna, the response of which is a function of MTM dimensions as well as of locations of MTM cells along the dipole arms. A prototype of the proposed miniaturized MTM-loaded printed dipole is fabricated to validate the

simulation results. A good agreement between the measured and simulated results is achieved

ACKNOWLEDGMENT

The authors would like to thank Iran Telecommunication Research Centre (ITRC) for its financial supports.

REFERENCES

- [1] S. D. Rogers, C. M. Butler, and A. Q. Martin "Design and Realization of GA-Optimized Wire Monopole and Matching Network With 20:1 Bandwidth," *IEEE Trans. Antennas Propag.*, vol. 51, no. 3, 493–502, 2003.
- [2] A. Erentok, P. Luljak, and R. W. Ziolkowski, "Antenna Performance Near a Volumetric

- Metamaterial Realization of an Artificial Magnetic Conductor,” *IEEE Trans. Antennas Propag.*, vol. 53, 160–172, 2005.
- [3] A. Jafargholi, M. Kamyab, M. Rafaei, and M. Veysi, “A Compact Dual-Band Printed Dipole Antenna Loaded with CLL-Based Metamaterials,” *International Review of Electrical Engineering*, vol. 5, no. 6, 2710-2714, 2010.
- [4] Q. Liu, P. S. Hall, and A. L. Borja, “Efficiency of Electrically Small Dipole Antennas Loaded with Left-Handed Transmission Lines,” *IEEE Trans. Antennas Propag.*, vol. 57, no. 10, 3009–3017, 2009.
- [5] A. Jafargholi, M. Kamyab, and M. Veysi, “Artificial Magnetic Conductor Loaded Monopole Antenna,” *IEEE Antennas Wireless Propag. Lett.*, vol. 9, pp. 211-214, 2010.
- [6] H. Iizuka, P. S. Hall, and A. L. Borja, “Dipole Antenna with Left-Handed Loading,” *IEEE Antennas Wireless Propag. Lett.*, vol. 5, 483–485, 2006.
- [7] A. L. Borja, P. S. Hall, Q. Liu, and H. Iizuka, “Omnidirectional Left-Handed Loop Antenna,” *IEEE Antennas and Wireless Propagation Lett.*, vol. 6, pp. 495-498, 2007.
- [8] H. Iizuka and P. S. Hall, “Left-Handed Dipole Antennas and Their Implementations,” *IEEE Trans. Antennas Propag.*, vol. 55, no. 5, pp. 1246–1253, 2007.
- [9] M. Rafaei Booket, M. Kamyab, A. Jafargholi, and S. M. Mousavi, “Analytical Modeling of the Printed Dipole Antenna Loaded with CRLH Structures,” *Progress In Electromagnetics Research B*, vol. 20, 167-186, 2010.
- [10] J. Zhu, M. A. Antoniadis, and G. V. Eleftheriades, “A Compact Tri-Band Monopole Antenna with Single-Cell Metamaterial Loading,” *IEEE Trans. Antennas Propag.*, vol. 58, no. 4, 1031–1038, 2010.
- [11] H. Mosallaei and K. Sarabandi, “Design and Modeling of Patch Antenna Printed on Magneto-Dielectric Embedded-Circuit Metasubstrate,” *IEEE Trans. Antennas Propag.*, vol. 55, no. 1, 1031–1038, 2007.
- [12] S. A. Tretyakov, S. I. Maslovski, A. A. Sochava, and C. R. Simovski “The Influence of Complex Material Coverings on the Bandwidth of Antennas,” *Physics. Class-ph*, 2004.
- [13] C. A. Balanis, *Advanced Engineering Electromagnetics*, Wiley, 1989.
- [14] N. Engheta and R. Ziolkowski, *Metamaterials: Physics and Engineering Explorations*, Wiley, 2006.
- [15] M. Veysi, M. Kamyab, S. M. Mousavi, and A. Jafargholi “Wideband Miniaturized Polarization-Dependent HIS Incorporating Metamaterials,” *IEEE Antennas Wireless Propag. Lett.*, vol. 9, 764-766, 2010.
- [16] V. Lucarini, J. J. Saarinen, K.-E. peiponen, and E. M. vartiainen, “Kramers-Kronig Relation in Optical Materials Research,” *Springer Series in Optical Sciences*, 2004.
- [17] Alu and N. Engheta; “Pairing an Epsilon-Negative Slab With a Mu-Negative Slab: Resonance, Tunneling and Transparency,” *IEEE Trans. Antennas Propag.*, vol. 51, pp. 2558–2571, 2003.
- [18] D. Sievenpiper, “Chapter 11: Review of Theory, Fabrication, and Applications of High Impedance Ground Planes,” in *Metamaterials: Physics and Engineering Explorations*, edited by N. Engheta and R. Ziolkowski, Wiley, 2006.
- [19] A. K. Iyer and G. V. Eleftheriades, “A Multilayer Negative-Refractive Index Transmission-Line Metamaterial Free-Space Lens at X-Band,” *IEEE Trans. Antennas Propag.*, vol. 55, no. 10, pp. 2746–2753, 2007.
- [20] D. L. Sounas, N. V. Kantartzis, and T. D. Tsiboukis, “Focusing Efficiency Analysis and Performance Optimization of Arbitrarily Sized DNG Metamaterial Slabs with Losses,” *IEEE Trans. Microw. Theory Tech.*, vol. 54, no. 12, 4111–4121, 2006.
- [21] A. Alù, F. Bilotti, N. Engheta, and L. Vegni, “Subwavelength, Compact, Resonant Patch Antennas Loaded with Metamaterials,” *IEEE Trans. Antennas Propag.*, vol. 55, no. 1, pp. 13-25, 2007.
- [22] N. V. Kantartzis, D. L. Sounas, and T. D. Tsiboukis, “Stencil-Optimized Time-Domain Algorithms for Compact Circular Patch Antennas with Anisotropic Metamaterial Substrates,” *IEEE Trans Magn.*, vol. 45, no. 3, 1368-1371, 2009.
- [23] M. Tang, S. Xiao, D. Wang, J. Xiong, K. Chen, and B. Wang, “Negative Index of Reflection in Planar Metamaterial Composed of Single Split-Ring Resonators,” *Applied Computational Electromagnetic Society (ACES) Journal*, vol. 26, no. 3, 250 – 258, 2011.
- [24] M. Naghshvarian-Jahromi and N. Komjani-Barchloui, “Analysis of the Behavior of Sierpinski Carpet Monopole Antenna,” *Applied Computational Electromagnetic Society (ACES) Journal*, vol. 24, no. 1, pp. 32 – 36, 2009.



Amir Jafargholi received the Ph.D. degree in Electrical Engineering from K.N. Toosi University of Technology, Tehran, Iran, in 2011. He is the coauthor of about 50 scientific contributions published in international books, journals and peer-reviewed conference proceedings. His research interest includes the applications of metamaterials in the analysis and synthesis of antennas.

Dr. Jafargholi was a recipient of a Student's Best Thesis National Festival award for his B.S. thesis, on May 2006. He was a recipient of the 22th Khawarizmi International and 13th Khawarizmi Youth Award on Jan. 2009 and Oct. 2011, respectively. He was also the recipient of Research Grant Awarded in Metamaterial 2010.



Manouchehr Kamyab received the B.S. and M.S. from the University of Tehran, Tehran, Iran, and the Ph.D. degree from Michigan State University, in 1982, in Electrical Engineering. His research interest includes the metamaterials and their applications in antenna engineering, electrically small antennas, microwave and millimeter-wave circuits, and mobile communication systems. He is currently an associate professor in the Department of Electrical Engineering, K.N. Toosi University of Technology, Tehran, Iran.

Dr. Kamyab is leading a group of graduate students in the areas of negative-refraction metamaterials and their microwave applications, integrated antennas and components for broad-band wireless telecommunications, novel antenna beam-steering techniques, millimeter and submillimeter-wave circuits, as well as scattering and inverse scattering problems.